This article has been accepted for inclusion in a future issue of this journal. Content is final as presented, with the exception of pagination.

A Hybrid Low-Cost Bandpass Filter With SAW Resonators and External Lumped Inductors Using a Dual-Coupling Scheme

Runqi Zhang, *Member, IEEE*, Mahmoud Abdelfattah, *Student Member, IEEE*, Li Yang, *Member, IEEE*, Roberto Gómez-García, *Senior Member, IEEE*, and Dimitrios Peroulis, *Fellow, IEEE*

***Abstract*— A class of hybrid low-cost bandpass filter (BPF) with only two kinds of circuit components, straightforward design procedure, and miniaturized circuit footprint is presented. The proposed BPF is based on a hybrid module composed of one type of surface-acoustic-wave (SAW) resonator and one external lumped inductor. Compared with traditional SAW-resonator-based BPF devices, the use of a single-SAW-resonator model for its design reduces the cost and complexity by avoiding the need for well-matched SAW-resonator pairs. The engineered filter topology consists of a dual-path coupling scheme, in which one coupling path is simply a series-type SAW resonator and another path is made up of two SAW resonators that are intercoupled by means of an external inductor in the middle. Such coupling architecture generates two additional transmission zeros (TZs) that allow to increase the out-of-band power-rejection levels and enlarge the stopband bandwidth. A circuit analysis based on the even-/odd-mode method is applied to derive its equivalent circuit that can be directly matched to a conventional transversal filter topology. The obtained equivalent circuit readily illustrates the operational mechanisms of the proposed filter principle in terms of reflection zeros and TZs. Subsequently, the quality factors of its even- and odd-mode-subnetwork resonators are analytically derived, and the obtained numerical results determine the tradeoff existing when choosing the external-inductor value among various performance metrics. For experimental validation purposes, two 418-MHz BPF prototypes formed by one and two in-series-cascade-connected second-order filtering units, respectively, are manufactured and tested. The circuit footprints of these filters are largely reduced by using a three-layer lamination technique for their physical implementations. The measured results show sharp-rejection filtering responses and are in close agreement with the theoretical predictions.**

***Index Terms*— Acoustic-wave filter, bandpass filter (BPF), hybrid acoustic and lumped elements, surface-acoustic-wave (SAW) resonator, transmission zero (TZ), transversal filter.**

Manuscript received September 5, 2019; revised December 27, 2019; accepted January 15, 2020. *(Corresponding author: Runqi Zhang.)*

Runqi Zhang was with Purdue University, West Lafayette, IN 47907 USA. He is now with Akoustis, Inc., Hunversville, NC 28078 USA (e-mail: rzhang1@e.ntu.edu.sg).

Mahmoud Abdelfattah was with Purdue University, West Lafayette, IN 47907 USA. He is now with Skyworks Solutions, Inc., Newbury Park, CA 91320 USA (e-mail: abdelfat@purdue.edu).

Li Yang and Roberto Gómez-García are with the Department of Signal Theory and Communications, Polytechnic School, University of Alcalá, 28871 Alcalá de Henares, Spain (e-mail: yang96507@gmail.com; roberto.gomez.garcia@ieee.org).

Dimitrios Peroulis is with the School of Electrical and Computer Engineering, Purdue University, West Lafayette, IN 47907 USA (e-mail: dperouli@purdue.edu).

Color versions of one or more of the figures in this article are available online at http://ieeexplore.ieee.org.

Digital Object Identifier 10.1109/TMTT.2020.2969390

I. Introduction

MICROWAVE bandpass filters (BPFs) implemented by means of microelectromechanical systems (MEMs) acoustic-wave resonators are crucial in modern wireless communication systems. They exhibit remarkable features in terms of the compact size and effective quality factor in an integrated design, and they are less prominent to undesired nonlinearity issues usually found in RF active filters [1].

One of the most-commonly discussed surface-acoustic-wave (SAW) BPF architectures is the ladder-type topology [2]. This filter structure consists of multiple replicas of series- and shunt-type SAW resonators. Each SAW resonator produces one reflection zero and one transmission zero (TZ), and the overall filtering response exhibits steep rejection slopes and large attenuation depths. A synthesis method for this type of SAW-resonator-based BPF is discussed in [3], which exploits the derivation of an in-line equivalent circuit of the ladder-type configuration [4], [5]. Nevertheless, it is well known that acoustic-wave resonators, due to the used materials and layouts, cannot be designed to have arbitrary effective coupling coefficients. This imposes limitations at the design level since the Butterworth Van-Dyke (BVD) circuit models for the SAW resonators resulting from the synthesis process cannot be flexibly determined. Besides, each SAW resonator in the ladder-type architecture can be different in order to optimize the passband and stopband characteristics. To further increase the number of TZs and augment the out-of-band power-rejection levels, a design technique using dual-shunt acoustic resonators was reported in [6] and [7]. Nevertheless, it requires accurate control of the resonant and antiresonant frequencies of the two shunt resonators, which increases the design complexity and the production cost of the overall SAW-resonator-based BPF. Fortunately, other design techniques have been proposed that allow reducing the number of distinct BVD models that are required in a single filter. One example of these approaches is the one based on loading an inductor with the shunt-type acoustic-wave resonator so that the resulting hybrid resonant module has an equivalent lumped-element circuit model in a BVD format. Accordingly, the motional frequency of this BVD model can be then modified through the loaded inductor. This extra inductor is commonly implemented by means of bonding wire, which connects the resonator to the ground [8]. Another typical example of using external components to simplify a ladder-type BPF design is to employ external inductors or capacitors to provide the appropriate external coupling [9]. Despite the inclusion of external components increases both the circuit size and the in-band insertion-loss level as drawbacks, some advantages are gained in terms of the bandwidth increase for more general transfer-function synthesis and lower design complexity and cost.

In a simple and low-cost BPF design, the hybrid technique consisting of combining acoustic-wave resonators and external lumped components is found to be suitable. Note that in classic SAW-resonator BPF schemes, the bandwidth is primarily limited by the achievable effective coupling coefficient in the acoustic-wave resonator. However, the parallel connection of an external inductor with the acoustic-wave resonator can effectively reallocate the antiresonant frequency to be far away from the passband. Hence, the bandwidth flexibility in the resulting filter device is gained. In the meanwhile, the hybrid resonator generates another TZ on the other side of the passband so that the selectivity can be increased. Using this method, single and multiband BPFs have been devised in [10] and [11], respectively, and they have demonstrated unprecedented levels of controllability for this type of filter in terms of bandwidth for the transmission band(s) and out-of-band rejection profile. This technique is then modified in [12] for its application in a lattice-type structure for wide-band acoustic-wave-resonator-based BPF design. Also, as demonstrated in [13], the addition of an extra capacitor apart of the inductor allows to also flatten the in-band group-delay profile of the filter for low-phase-distortion purposes. Nevertheless, all the aforementioned hybrid-SAW-resonator/lumped-element BPF designs suffer from some major drawbacks, such as the addition of at least one external component per acoustic resonator that ultimately results in larger footprint and increased in-band insertion-loss levels. In addition, the inductor together with the acoustic-wave resonator can be viewed as a band-stop structure, causing some undesired spurious transmission bands due to flyback effects. To counteract these unwanted spurious bands, hybridized SAW-element/inductor resonators and fully lumped-element resonators can be combined together in the same filtering device as in [14] but at the expense of increased insertion-loss levels and larger circuit size.

Another major advantage of hybrid SAW-resonator/lumped-element BPF design techniques is that the out-of-band rejection levels can be further enlarged by introducing some advanced coupling schemes. For example, parasitic effects, such as packaging and wire bonding, can be exploited for this purpose by creating cross coupling as discussed in [15]. Cross coupling among SAW resonators can also be intentionally produced by adding extra capacitors and inductors, as demonstrated in [16]. In [17], it is verified that the mutual coupling between external inductors can help to improve the depth of a TZ. However, these techniques normally imply increased difficulty in the design procedure, by either more complicated equivalent circuits or time-lengthy processes to obtain the optimum design variables.

Other hybrid techniques combine acoustic-wave resonators (and even complete on-chip acoustic-wave BPFs) with other microwave elements, such as microstrip lines [18]. This design strategy takes benefit of the achievable broadband transmission characteristics of microstrip filters and the steep rejection slope inherent to the SAW element to realize SAW-filter-selectivity-like mixed-technology broadband BPFs. One example of such type of approach is discussed in [19], where intercascaded hybrid low-pass and high-pass filtering units based on the parallel connection of SAW resonators and transmission lines produce the BPF response. The filter in [20] exploits signal-interference concepts with in-series-cascaded hybrid SAW-resonator/microstrip transversal filtering sections to realize a sharp-rejection wide-band BPF. The major drawback of this kind of hybridized filter structure is its large circuit size, which is primarily occupied by the transmission-line part.

In this article, a low-cost BPF with hybrid SAW resonators and lumped inductors is proposed. This new filter topology is based on a dual-path coupling scheme, in which one coupling path consists of an in-series SAW resonator and the other path is composed of two cascaded SAW resonators that are intercoupled through an external shunt-type inductor. The application of the even-/odd-mode analysis in Section II to this filtering module reveals that each coupling path introduces one resonance within the passband range to conform to a two-pole transmission band. In addition, their parallel connection creates one TZ, whereas another extra TZ is produced from the capacitive source-load coupling existing in its equivalent circuit network. Despite utilizing three SAW resonators to realize a second-order BPF, the proposed coupling scheme avoids the use of cross couplings among the main SAW resonators that are usually sensitive to get extra TZs. The dual-coupling scheme is next analyzed in terms of the quality factor of the obtained even- and odd-mode-subnetwork resonators. This process matches the hybrid SAW-element/inductor filtering block with transversal filter architecture so that its operational principle can be readily explained by means of well-established filter design theory. From this study, the trade-off existing when selecting the inductor value is accordingly discussed. For experimental demonstration purposes, two filter prototypes made up of one single- and two second-order in-series-cascaded filtering units, respectively, are developed and characterized in Section III. Both filters are manufactured in a laminated three-layer layout to minimize their circuit sizes. Compared with conventional SAW-resonator-based or hybrid BPF designs that are available in the technical literature, the engineered BPF concept has the following merits.

1) It employs a single-SAW-resonator BVD model unlike in multi-SAW-resonator-based BPFs, hence effectively lowering the cost of the design, optimization, and fabrication processes.
2) It only requires a single external inductor per two-pole filtering block, thus minimizing the negative effects associated with extra lumped elements in terms of increased circuit footprint and in-band insertion-loss levels.
3) It is implemented in a laminated circuit layout to further reduce the overall circuit size.

II. Hybrid Filter Analysis

The proposed hybrid SAW-resonator/lumped-inductor filtering module is discussed in detail in this section.

This article has been accepted for inclusion in a future issue of this journal. Content is final as presented, with the exception of pagination.

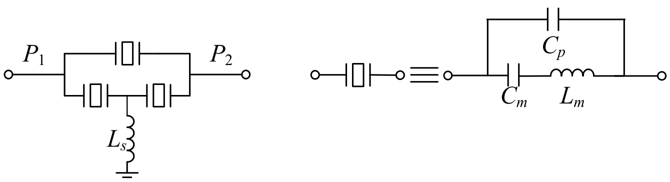

Fig. 1. Proposed hybrid filter structure, where the SAW resonator is represented by its lossless BVD model (the BVD model has the following component values: $C_p = 1.579$ pF, $C_m = 1.1$ fF, and $L_m = 131.8$ uH).

First, the devised filtering block is analyzed by means of the even-/odd-mode method to match it to its equivalent transversal circuit. This obtained equivalent circuit is then used to demonstrate the operational principle of the devised hybrid filter in terms of reflection zeros and TZs. Subsequently, the study of the quality factors of the resonators associated with its even- and odd-mode-subnetworks is presented. As a result of this analysis, design considerations to be evaluated when choosing the value of the external inductor are derived. In the end, the hybrid filter design procedure is discussed in detail. Note that, throughout this article, a SAW resonator model ASR418S2 from Abracon with a main resonant frequency at 418 MHz that features unloaded and loaded quality factors of 10 730 and 1400, respectively, is considered. For the sake of simplicity, the SAW BVD equivalent circuit that only models the main motional resonant branch is assumed [21], i.e., narrowband model, so that the spurious modes are not represented by it. In addition, when analyzing the quality factor of the hybrid filter block, the loss dissipated in the SAW resonator is regarded as the one dominantly coming from the resistor in the motional branch, in accordance with the information provided by the datasheet of the SAW-resonator model used in the filter prototypes that are developed and tested in Section III. Although modified BVD models as in [22] that include a second resistor in series with the parallel capacitor may more closely match the resonator response, they are not considered here for the sake of simplicity. Nevertheless, the proposed analysis can be readily extended to more complex modified BVD models without loss of validity.

A. Transversal Equivalent Circuit of the Hybrid Filter

The proposed hybrid filter architecture is shown in Fig. 1, which is composed of three SAW resonators and one external lumped inductor L_s. The three SAW resonators are represented by the same lossless BVD model, which is made up of the motional capacitor and inductor in an in-series main branch, C_m and L_m, respectively, and a parallel capacitor C_p. The overall filter structure is based on a dual-path coupling scheme, where the first path is simply a series-type SAW resonator, and the second one consists of two in-series-cascaded SAW resonators that are intercoupled by the inductor L_s. This dual-path coupling topology, whose operational foundations are described in the following, is expected to produce two reflection zeros and two TZs to create a two-pole quasi-elliptic-type filtering transfer function.

Given the symmetry property of this filter topology, the even-/odd-mode technique can be readily employed for its

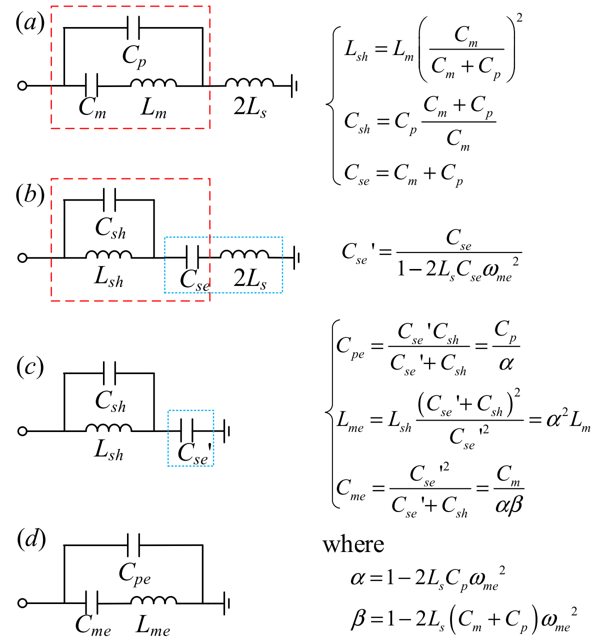

Fig. 2. Even-mode bilateral circuit and its sequentially derived equivalent circuits (the component values are derived in a step-by-step manner as shown beside the figure). (a) Circuit of the SAW BVD model and the inductor. (b) Transformation of the BVD model to its equivalent in the red dash box. (c) Correspondence of the circuit in the blue dot box with a single capacitor. (d) Transformation of the circuit back to a BVD circuit.

theoretical analysis. When an even excitation is applied at ports 1 and 2, it gives rise to the bilateral circuit depicted in Fig. 2(a). To unearth the effect of the loaded inductor, the SAW BVD model (in the red dashed box) is transformed to the equivalent network shown in Fig. 2(b). Next, the inductor $2L_s$ is combined with C_{se} (in blue dotted box), and they are represented by a new equivalent capacitor C_{se} in the blue dashed box in Fig. 2(b) and (c). It should be noticed that this equivalence is only perfect at a single frequency, i.e., the resonant frequency of the even-mode f_{me} or simply the main in-series resonant frequency f_m of the SAW element. The intermediate circuit (in purple dashed-dotted box) can now be converted back to a BVD circuit, as detailed in Fig. 2(d). Following this procedure, all the component values in the BVD circuit can also be obtained, as listed in Fig. 2. In this manner, the even-mode resonating circuit is fully derived.

It is interesting to note that the component values in Fig. 2(d) are scaled by a linear factor of α and β compared with the original SAW-resonator BVD model. Accordingly, the even-mode-subnetwork resonator has modified motional and antiresonant angular frequencies ($\omega_{(me,pe)}$) given by

$$\begin{cases} \omega_{me}^2 = \dfrac{1}{L_{me}C_{me}} = \dfrac{\beta}{\alpha}\omega_m^2 \\ \omega_{pe}^2 = \left(\dfrac{1}{C_{pe}} + \dfrac{1}{C_{me}}\right)\dfrac{1}{L_{me}} = \dfrac{\beta C_p + C_m}{\alpha(C_p + C_m)}\omega_p^2 \end{cases} \tag{1}$$

where $\omega_{(m,p)}$ are the motional and antiresonant angular frequencies of the constituent SAW resonator, respectively.

From the previous study, some conclusions can be drawn. First, as the inductor L_s is increased, the ratio β/α decreases, and it results in a smaller resonant angular frequency ω_{me}.

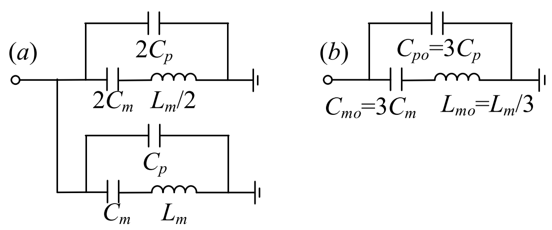

Fig. 3. Odd-mode bilateral circuit and its equivalent circuit. (a) Odd-mode bilateral circuit from the SAW BVD models. (b) Equivalent BVD circuit.

Meanwhile, the antiresonant angular frequency ω_{pe} is almost unchanged since $C_p \gg C_m$ and the factor β/α becomes close to the unity. However, it should be highlighted that the above-mentioned analysis assumes that the loaded inductor L_s is small enough such that $2L_s$ in combination with C_{se} [the blue dashed box in Fig. 2(b)] is in general capacitive. At a higher frequency, the cascaded connection of L_s and C_{se} indeed generates a resonance as a result of their reactance compensation. At this time, the derived equivalent even-mode BVD circuit is not valid due to its narrowband nature. These two resonances ($\omega_{me(1,2)}$), i.e., the even-mode resonance and its spurious, can be determined as

$$j\omega L_{me} + \frac{1}{j\omega C_{me}} = 0 \rightarrow \omega_{me(1,2)}{}^2 = \frac{a \pm \sqrt{a^2 - 2b}}{b} \quad (2a)$$

where

$$\begin{cases} a = 2L_s(C_m + C_p) + L_m C_m \\ b = 4L_s C_p L_m C_m. \end{cases} \quad (2b)$$

The odd-mode analysis is relatively simple as the virtual ground in the symmetry plane shortens the inductor L_s, leading to two sets of short-circuited stubs, as shown in Fig. 3(a). These two sets of stubs can be combined in a BVD circuit, which results in the formation of the odd-mode-subnetwork resonator shown in Fig. 3(b). Although the component values in Fig. 3(b) are scaled with regard to those of the original SAW BVD model, the motional resonant and antiresonant frequencies remain unchanged.

Both the even- and odd-mode-analyses result in the derivation of their equivalent BVD circuit models, as shown in Figs. 2(d) and 3(b), respectively. These two circuits can be transformed back to the filter scheme detailed in Fig. 4(a), which has the same even- and odd-mode bilateral circuits. To separate different even- and odd-mode excitations, a transformer pair with the opposite phase is added for the even-mode excitation, and a transformer pair with the same phase is considered for the odd-mode excitation. The obtained filter can be further represented by the transversal filter structure depicted in Fig. 4(b). The transformer pairs are replaced by admittance inverters, and the series-type resonators are changed by shunt-type resonators. The parallel capacitors ($C_{p(e,o)}$) are grouped together into a Π-shaped capacitive network. The detailed analysis of such transversal structure is discussed in [23], and it can readily illustrate the operational mechanism of the proposed hybrid filter. The two transversal modes, i.e., the even and odd modes, produce two reflection zeros and one TZ. Since the even-mode resonant frequency is

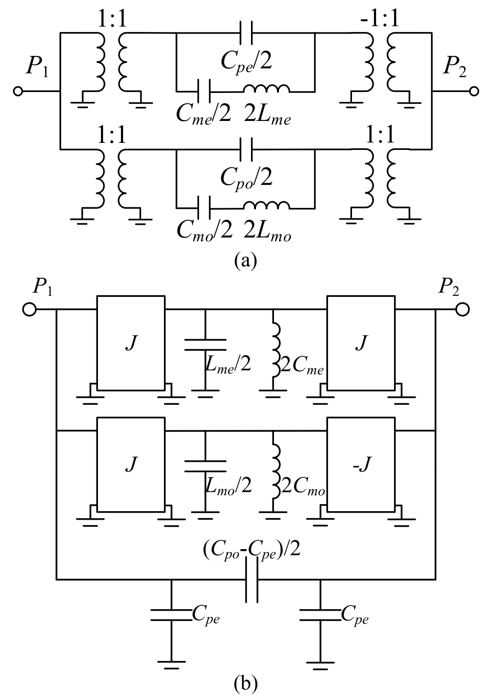

Fig. 4. (a) Combination of the even- and odd-mode subnetwork resonators to form the equivalent circuit of the hybrid filter. (b) Equivalent transversal filter.

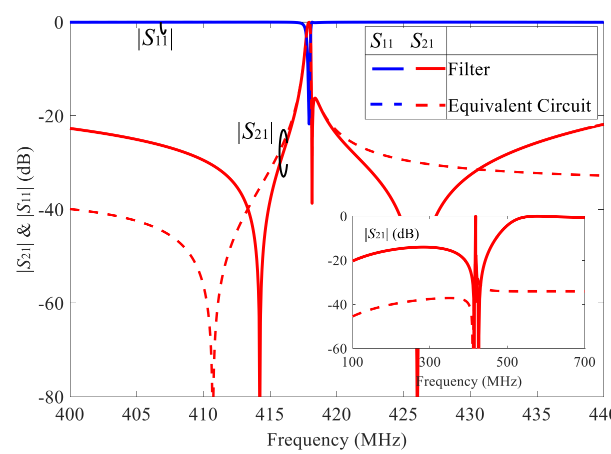

Fig. 5. Example comparison of two counterpart filtering responses associated with the proposed hybrid filter in Fig. 1 and its equivalent circuit in Fig. 4, respectively (the values of the SAW BVD model elements were given in the caption of Fig. 1, and the external inductor is L_s = 30 nH so that the obtained values for the elements of the equivalent circuit are C_{pe} = 4.56 pF, C_{me} = 0.92 fF, L_{me} = 15.82 uH, C_{po} = 4.74 pF, C_{mo} = 0.33 fF, and L_{mo} = 43.93 uH).

lower than the odd-mode one, this TZ is allocated at the lower side of the passband [24]. The Π-shaped capacitive network implements a source-load coupling that generates another TZ at the upper side of the passband [23]. Thus, a total of two reflection zeros and two TZs are created by this filter network so that a two-pole quasi-elliptic-type filtering transfer function is theoretically obtained.

As a verification of the above discussion, an example comparison between two counterpart filtering responses associated with the circuit networks shown in Figs. 1 and 4, respectively, is shown in Fig. 5. As can be seen, the transfer function of the equivalent transversal filter structure closely matches one of the initial hybrid filters in the proximities of the passband, which shows two reflection zeros and two TZs as theoretically expected. However, for frequencies far away from the passband range, the two filtering responses are different due to the narrowband nature of the derived transversal circuit equivalent. This also refers to the spurious resonance present in the hybrid filter, which is not included or ignored by its equivalent transversal circuit. In particular, this spurious resonance in Fig. 5, as calculated by (2), is approximately located at around 600 MHz for a center frequency of around 400 MHz. Although the presence of the spurious resonance deteriorates the out-of-band rejection levels at spectral regions far away from the main passband, it contributes to the creation of a third TZ at about 426 MHz, which serves to further enhance the upper close-to-passband attenuation levels.

B. Quality Factors of the Transversal Resonant Modes

An important consideration in hybrid filter design, although also usually ignored or omitted by available design techniques for these classes of mixed-technology filters, is the quality factor. By definition, the quality factor of a resonating circuit is a ratio between the stored energy and the average dissipated power. A classic method to calculate the unloaded quality factor (Q_u) uses the impedance phase slope as follows [25]:

$$Q_u = \frac{f}{2}\left(\frac{d\phi_z}{df}\right)|_{f=f_r} \tag{3}$$

where ϕ_z is the input impedance phase of the resonating circuit and f_r is the resonant frequency. Depending on the resonating circuit, the resulting analytical expression from (3) can be very complex when using [26] so that a numerical calculation is mostly preferred. However, such numerical computation treats any resonator as a simplified *LC* model. Consequently, it fails to provide in-depth information regarding the physical architecture and/or physical phenomena associated with the resonating circuit under analysis.

In a hybrid filter design, as the one proposed in this work, the SAW resonators exhibit relatively high-quality factors, while the external inductor has a much lower one. In this manner, it is the external-inductor element that reduces the quality factor of the equivalent even-mode-subnetwork resonator, as demonstrated in the following. At the resonant frequency, the amount of stored energy and dissipated power is distributed within both the SAW resonator and the external inductor. To analyze the quality factor and the dissipated power of each part in the hybrid filter design, the following approximate conditions are assumed.

1) The lossy SAW resonator only includes one resistor in the motional branch, and the lossy inductor model has one series resistor as illustrated in Fig. 6(a).
2) The stored electric and magnetic energies ($W_{(e,m)}$) are equal at the resonant frequency so that the total stored energy is $W_e + W_m = 2W_e = 2W_m$. Following this argument, the stored energy in an *LC* resonant tank is $W_e + W_m = CV^2/2 = LI^2/2$ ($W_e = CV^2/4 = W_m = LI^2/4$), where V and I are the peak voltage and current across the circuit component, respectively.

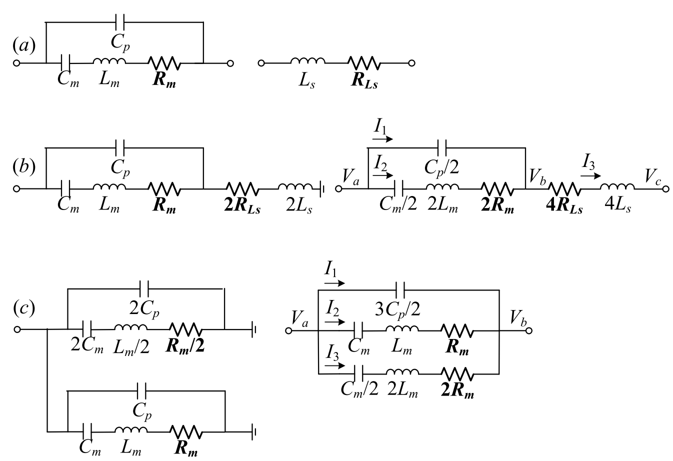

Fig. 6. Lossy circuits employed to analyze the quality factors. (a) SAW-resonator and inductor models, including the resistors. (b) Resistor-included even-mode bilateral circuit and equivalent even-mode subnetwork resonator. (c) Resistor-included odd-mode bilateral-circuit and equivalent odd-mode subnetwork resonator (the component values of the SAW resonator are $C_p = 1.579$ pF, $C_m = 1.1$ fF, $L_m = 131.8$ uH, and $R_m = 28\ \Omega$; the frequency value for the calculation is chosen at the resonant frequency f_{me} of the overall resonator).

3) The cases for the equivalent even- and odd-mode subnetwork resonators in Fig. 6(b) and (c), respectively, are analyzed separately.

First, the even-mode bilateral circuit shown in Fig. 2(a) corresponding to the proposed hybrid SAW-resonator/inductor filtering block in Fig. 1 is modified to include the resistors in the SAW BVD model and the inductor, as detailed in Fig. 6(b). The equivalent even-mode-subnetwork resonator is then accordingly derived, and its quality factor is analyzed based on this circuit topology. The three circuit nodes in Fig. 6(b) have the voltages of $V_{(a-c)}$, respectively, which drives the currents $I_{(a-c)}$ in the three stubs of the input admittance $Y_{\text{in}(1-3)}$. Therefore, the voltage relates to the current as

$$\begin{cases} I_1 = (V_a - V_b)Y_{\text{in}1} \\ I_2 = (V_a - V_b)Y_{\text{in}2} \\ I_3 = I_1 + I_2 \end{cases} \tag{4a}$$

where

$$\begin{cases} Y_{\text{in}1} = j\omega\dfrac{C_p}{2} \\ Y_{\text{in}2} = \dfrac{1}{j\omega 2L_m + \frac{2}{j\omega C_m} + 2R_m} \\ Y_{\text{in}3} = \dfrac{1}{j\omega 4L_s + 4R_{Ls}}. \end{cases} \tag{4b}$$

In each stub, the capacitor and the inductor store the energy $W_{(e,m)x}$, respectively, and the resistor dissipates the power P_{rx} (x = 1, 2, and 3). When calculating the loaded quality factor, the port impedances are deemed to dissipate the power P_{SL}.

The stub 1 (conducting current I_1) only contains a capacitor and no resistor so that its stored energy is calculated as

$$W_{e1} = \frac{1}{4}|V_a - V_b|^2\frac{C_p}{2}. \tag{5a}$$

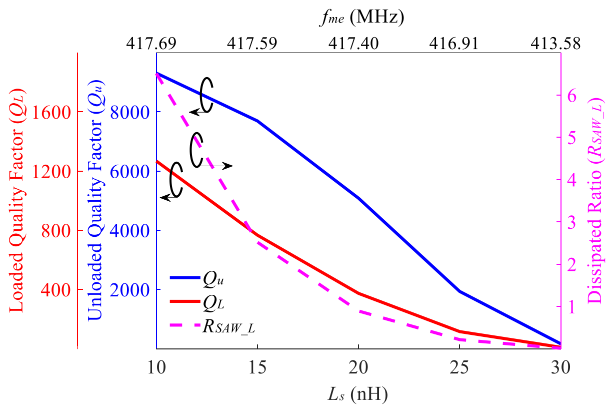

Fig. 7. Loaded (Q_L) and unloaded (Q_u) quality factors of the equivalent even-mode-subnetwork resonator as a function of the external inductor value L_s (f_{me} is the resonant frequency of the even-mode-subnetwork resonator, and the external inductor is assumed to have an unloaded quality factor of 50).

The stub 2 (conducting current I_2) models the motional resonance and contains a resistor so that the stored energies and dissipated power are computed as

$$W_{m2} = \frac{1}{4}|I_2|^2 2L_m, \quad W_{e2} = \frac{1}{4}|V_{C2}|^2 \frac{C_m}{2}, \quad P_{r2} = \frac{1}{2}|I_2|^2 2R_m. \tag{5b}$$

The stub 3 (conducting current I_3) corresponds to the lossy inductor, and its stored energy and dissipated power are

$$W_{m3} = \frac{1}{4}|I_3|^2 4L_s, \quad P_{r3} = \frac{1}{2}|I_3|^2 4R_{Ls}. \tag{5c}$$

The port characteristic impedance consumes the power as follows:

$$P_{SL} = \frac{1}{2}|I_3|^2(R_S + R_L). \tag{5d}$$

From the above-mentioned derivations, the loaded and unloaded quality factors at the resonant angular frequency of the even mode ω_{me} in (1), Q_u and Q_L, respectively, are, thus, calculated as follows:

$$Q_u = \omega\frac{\sum_{i=1}^{3}(W_{ei} + W_{mi})}{\sum_{i=1}^{3} P_{ri}}, \quad Q_L = \omega\frac{\sum_{i=1}^{3}(W_{ei} + W_{mi})}{P_{SL} + \sum_{i=1}^{3} P_{ri}}. \tag{6a}$$

The dissipated-power ratio between the SAW part and the inductor ($R_{\mathrm{SAW}-L}$) can be then obtained as follows:

$$R_{\mathrm{SAW}\_L} = \frac{P_{r2}}{P_{r3}}. \tag{6b}$$

A plot of the numerical values of the calculated unloaded and loaded quality factors through (6a) is shown in Fig. 7. As can be seen, as the inductor value increases, the resonant frequency associated with the even-mode-subnetwork resonator gets lower. However, the quality factors also drop dramatically. This is because the amount of dissipated power in the lossy inductor gets higher so that the ratio $R_{\mathrm{SAW}-L}$ drops accordingly. This means that a large inductor cannot be used to modify the resonant frequency since it results in lower quality factors [27].

A similar method can be applied for the odd-mode-subnetwork analysis, as shown in Fig. 6(c). The resistors in the odd-mode-subnetwork resonator are mainly distributed in the two motional branches, and their ratio with regard to the motional inductor in their respective branches is the same. As the majority of the energy is stored in the motional branch, the parallel capacitor has little impact on the calculation of the quality factors. It is then concluded that the odd-mode-sub-network resonator exhibits the same quality factor as the SAW BVD model.

C. Hybrid Filter Design

The design of the proposed hybrid filter module shown in Fig. 1 is based on the selection of its two different building circuit elements: the SAW resonator and the external inductor. The motional resonance of the SAW resonator can be chosen as close as possible to the desired center frequency for the overall passband, and the antiresonant frequency (or, equivalently, the effective coupling coefficient) approximately determines the achievable bandwidth.

The choice of the external inductor has to consider the following tradeoff derived from the analysis expounded in Section II-B. First, a larger value for the external inductor results in the reduction of the resonance frequency associated with the even-mode-subnetwork resonator so that the achievable filter bandwidth is increased. However, a large inductor with high-quality factors may be difficult to find/implement. Nevertheless, in the devised hybrid filter module, the combination of the SAW elements and the inductor gives rise to a reduction of the quality factors of the even-mode-subnetwork resonator with regard to the one inherent to the SAW element itself. This leads to an increase in the in-band insertion loss of the total filter. Moreover, additional considerations must be evaluated in terms of out-of-band power-rejection levels. Specifically, increasing the inductor value moves the TZ allocated at the lower side of the passband far away from it. Consequently, in the resulting quasi-elliptic-type two-pole filtering transfer function of the hybrid filter module, the TZ modification can improve/deteriorate the rejection slope at the expense of decreasing/increasing the out-of-band attenuation levels at frequencies far away from the passband. This is illustrated in Fig. 8 with some example responses. In summary, the selection of the inductor value must be done accordingly to these design rules related to the desired bandwidth, effective quality factor that ultimately determines the in-band insertion-loss levels, and out-of-band rejection profile.

Regarding the in-band characteristics, note that the proposed hybrid filter has only two different types of circuit components and a simple coupling scheme. As such, it seems to provide little freedom in controlling the coupling coefficient to shape the desired passband. Nevertheless, as revealed by the results in Fig. 8, the passband width can be enlarged as the external-inductor value is increased due to the previously referred lower-TZ-reallocation effect for the same type of acoustic resonator (note that larger coupling-coefficient SAW elements as in [9] can also be exploited in this hybrid SAW-resonator/lumped-inductor BPF architecture for larger

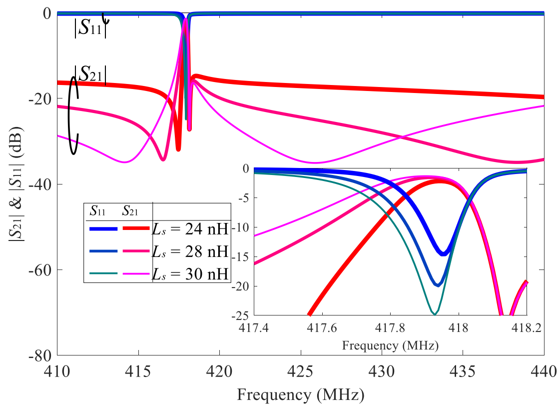

Fig. 8. Comparison between the hybrid-filter responses in terms of power transmission ($|S_{21}|$) and reflection ($|S_{11}|$) parameters for different inductor values (these responses are obtained with the lossy SAW BVD model and an inductor with unloaded quality factor of 50; the even-mode-subnetwork resonator has an unloaded quality factor, as found with the graphs shown in Fig. 7, equal to 2529, 581, and 165, respectively, whereas the obtained 3-dB bandwidths are 0.16, 0.2, and 0.24 MHz).

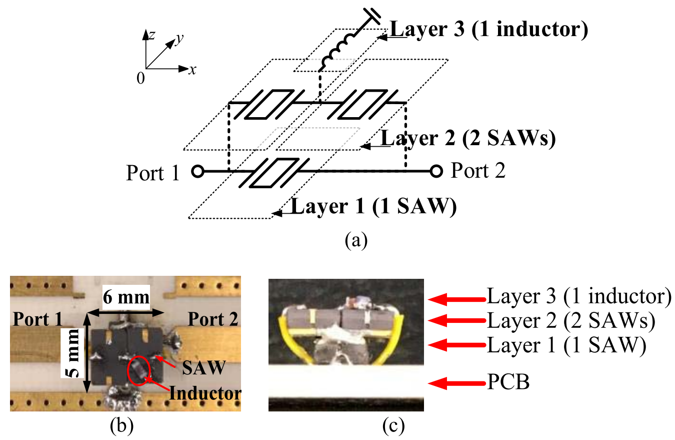

Fig. 9. Layout of the laminated single-stage hybrid filter prototype. (a) 3-D schematic view. (b) Top view of the implemented filter prototype. (c) Side view of the implemented filter prototype.

bandwidth realizations). In addition, some techniques can be used to adjust the in-band ripple profile as desired. For example, in the dual-coupling scheme or signal-interference circuit, the addition of shunt-type inductive or capacitive components at the input and output terminals can be adapted to alter the coupling coefficient, as proven in [28]–[30]. As an alternative method, the approach in [19] exploits cascaded SAW resonators in order to change the reactance slope with regard to the one of the single-SAW resonator. When intercascaded SAW resonators replace one of the SAW resonators at the two sides of the external inductor in Fig. 1, an asymmetrical filter scheme is obtained. This topology allows altering the coupling coefficient so that the achievable bandwidth is modified. Following a similar procedure to the one reported in [13], a capacitor can be placed in shunt connection besides the inductor. In this way, the in-band response can be maintained, while the TZ position at the lower side of the passband can be modified. Furthermore, most of the referred techniques can be combined for more flexible designs although they are not addressed here for simplicity.

III. Experimental Results and Discussion

For practical demonstration purposes, two filter prototypes centered at 418 MHz have been developed and measured. The first one directly implements the single filtering unit shown in Fig. 1, and the second one is composed of the in-series-cascade connection of two replicas of this filtering unit for higher selectivity realization. Both BPF circuits use a three-layer laminated technique in their physical prototyping that greatly reduces their footprint. To better predict the filter responses, a chip of the single building SAW resonator was characterized separately, and the obtained measured S-parameters were employed in the simulation and optimization processes of both BPF circuits. Specifically, three sets of filtering responses are represented for each BPF prototype as follows: the BVD model-based simulation, the circuit simulation, and the measurement. The employed external inductor is from the Coilcraft 0805HP series, the SAW-resonator chip is Abracon ASR418S2, and the trimmer capacitor is Knowles JZ060.

A. Single-Stage Filter

The single-stage filter prototype corresponds directly to the circuit schematic shown in Fig. 1, but it uses a three-layer lamination technique for its implementation, as seen in its conceptual layout given in Fig. 9(a). The first layer (layer 1) in the lamination only contains a SAW resonator, the second layer (layer 2) has two SAW resonators, and the third layer (layer 3) includes the external inductor. The packaged SAW resonators are connected through their input and output ports, while the remaining ports are internally connected as nonsignal ports. In a more conventional single-layer circuit, these nonsignal ports are usually shortened to the ground separately. In this case, they are mutually connected and shortened to the ground together via the nonsignal ports at the bottom layer (layer 1). The inductor in the top layer (layer 3) can touch any nonsignal port in layer 2 for grounding. Since the layer 2 circuit part exhibits wider length than the layer 1 circuit part, a jump wire is used to connect the SAW resonators between these two layers. Fig. 9(b) and (c) shows the top and cross views of the developed single-stage filter prototype. It should be noticed that although the laminated technique allows miniaturizing the overall circuit volume, it creates some unavoidable parasitic effects, such as the jump wire or the mutually connected nonsignal ports. However, these undesired parasitic effects can be partially compensated by changing the value of external inductor.

The BVD model, simulated, and experimental results in terms of power transmission, reflection, and in-band group-delay parameters for the single-stage filter prototype shown in Fig. 9 are depicted in Fig. 10 for two different inductor cases (values of 11 and 18 nH). As shown in Fig. 8, the inductor component with larger inductance value moves the TZ allocated at the lower side of the passband closer to it, hence increasing the rejection slope at this passband side. However, there is a tradeoff in terms of power-rejection

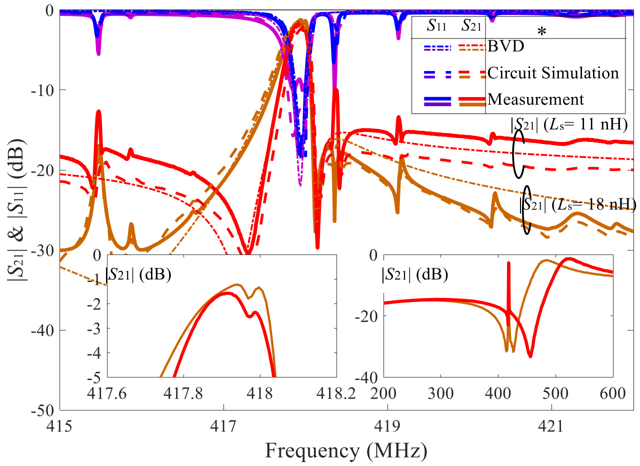

(a)

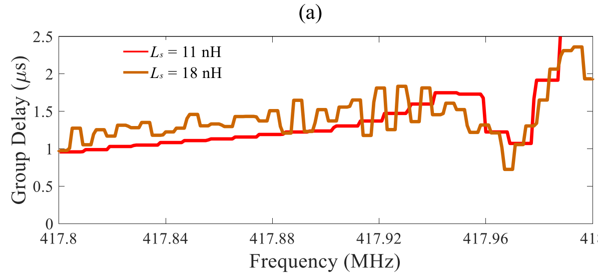

(b)

Fig. 10. (a) Power transmission ($|S_{21}|$) and reflection ($|S_{11}|$) responses obtained from the BVD model-based circuit, circuit simulation with the measured SAW-resonator S-parameters, and measurements of the single-stage hybrid filter prototype (two implementations with two different inductors are shown herein, and their responses are obtained with the lossy SAW BVD model and an external inductor with unloaded quality factor of 50; for each pair of lines in the legend, the upper lines are the case of $L_s = 11$ nH and the lower lines are $L_s = 18$ nH). (b) Measured in-band group-delay response of the single-stage hybrid filter prototype (for a clear view, especially the demonstration of the impact from the in-band spike, the measured group delay has been averagely processed).

levels at frequencies near and far away from the transmission band. For example, the smaller inductor case exhibits smaller rejection levels at 415 and 421 MHz but more attenuation at frequencies 417 MHz. On the other hand, the larger inductor case results in slightly wider bandwidth and closer spurious passbands. For these two measured smaller and larger inductor cases, the center frequency is 417.9 MHz, whereas the minimum in-band power-insertion-loss levels are around 1.3 and 1.5 dB, the 3-dB bandwidths are about 0.11 and 0.15 MHz, and the maximum in-band group-delay variations are equal to 1 and 2.1 μs, respectively. It is noted that the vertically laminated implementation solution adopted for this prototypes may introduce some undesired parasitic effects or couplings, such as those associated with the jumping wire to connect the SAW resonators in layers 1 and 2, an improper grounding for the circuit components in layer 2 and 3, and the cross coupling appearing among these components. These factors may produce some unexpected phenomena, such as the small in-band spikes observed around 417.9 MHz and the increase of the in-band insertion-loss level, as shown in Fig. 10. However, by means of proper packaging design, these undesired effects can be counteracted to a large extent.

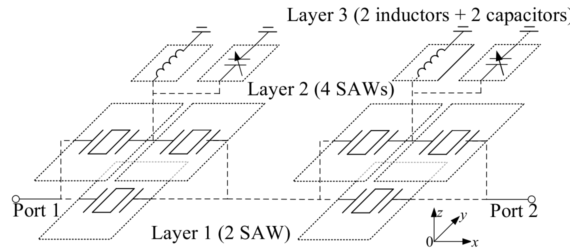

(a)

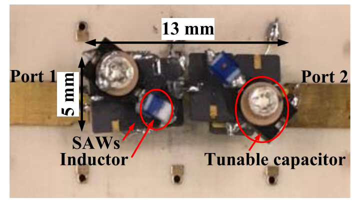

(b)

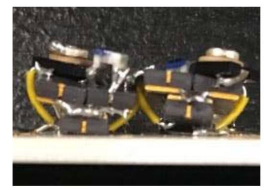

(c)

Fig. 11. Layout of the vertically laminated dual-stage hybrid filter prototype. (a) 3-D schematic view with the inclusion of extra capacitors for tuning purposes. (b) Top view of the implemented filter prototype. (c) Side view of the implemented filter prototype.

B. Dual-Stage Filter

The second developed prototype corresponds to a dual-stage filter composed of two in-series-cascaded replicas of the previous single-stage filtering unit so that its selectivity and out-of-band power-rejection levels can be increased. Fig. 11(a) and (b) shows the top and side views of the implemented filter circuit. External inductors with 24-nH inductance were selected for it. Since the inductor-value variation may have an impact on the overall filtering response, mechanically tunable capacitors were used in parallel with the inductors to slightly modify the inductor values and help to also compensate for the undesired effects coming from the manufacturing. These trimmer capacitors are placed on layer 3. It is noted that the added trimmer capacitor has little impact on the quality factor of the hybrid resonator and, hence, the in-band insertion loss of the filter. This is due to the fact that the majority of the energy is stored in the motional branch of the SAW resonator, and the capacitor normally exhibits a much higher quality factor than the inductor.

The BVD model, simulated, and experimental results in terms of power transmission and reflection parameters of the manufactured dual-stage filter prototype are shown in Fig. 12. Due to the two-unit cascading process, the rejection levels at frequencies beyond the TZs tend to reach 40 dB but at the expense of higher minimum insertion loss of 4.3 dB in a passband with a 3-dB bandwidth of about 0.12 MHz. The maximum group-delay variation within the measured 3-dB bandwidth is equal to 5 μs. Note also that the out-of-band rejection levels of the measured results at lower frequencies are larger than those predicted by the BVD circuit-based simulation. This can be attributed to the narrowband nature of the employed BVD model that only considers the primary resonance but not the spurious ones that serve to improve the rejection levels in the measured transfer function.

TABLE I

OMPARISON WITH SOME HYBRID SAW FILTERS

Reference*[1]	Technology*[2]	f_0/BW*[3] (MHz)	Order	Q_{eu}*[4]	$IL/Rej(1,2,4)$*[5] (dB)	Size (mm×mm)
[19](1)	SAW (×2) Transmission line (×3)	2000/400	---	(282, 903)	0.5/(20, 30, 30)	25×40
[10](2)	SAW (×1) SMD inductors (×2) SMD capacitor (×2)	418/1.0	2	(1525, 5150)	1.15/(10, 15, 30)	12.3×20.5
[9](1)	LWR (×2) On-chip inductors (×1) On-chip capacitors (×1)	142/1.25	12	2043	2.78/(45, 45, 45)	3×1.5
[30](2)	CMR (×1) On-chip inductors (×4)	498/2.1	3	1600	5.0/(15, 25, 40)	8×9
[31](2)	SHWR (×1) SMD inductors (×2) SMD capacitor (×2)	360/0.27	---	---	3.9/(25, 45, 65)	3×3
This work(2)	**SAW (×1) SMD inductor (×1)**	**418/0.12**	**4**	**2500**	**4.3/(15, 25, 38)**	**5×13**

1. The number after the reference indicates which experimental filter implementation is used for comparison.
2. SMD: surface-mount device; LWR: lamb wave resonator; CMR: contour-mode resonator; the number in the bracket shows how many different models of such circuit element are required; SHWR: shear horizontal wave resonator.
3. f_0: center frequency; BW: absolute 3-dB bandwidth.
4. Q_{eu}: range of unloaded quality factors for all the (hybrid) SAW resonators;
5. IL: insertion loss; Rej: out-of-band rejection at a frequency of interest; the number (1,2,4) after Rej represents a spectral distance from the center frequency equal to one, two, and four times the passband bandwidth.

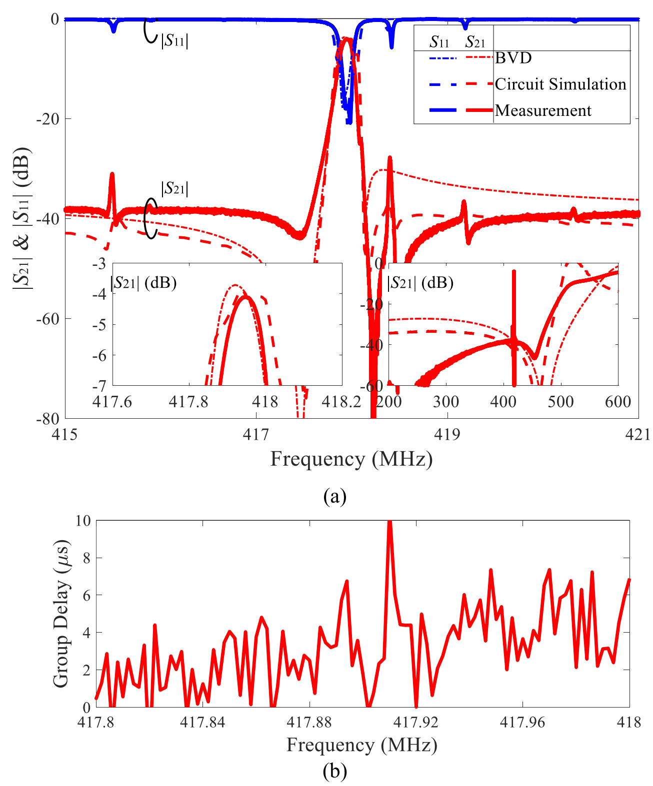

Fig. 12. (a) Power transmission ($|S_{21}|$) and reflection ($|S_{11}|$) responses obtained from the BVD model-based circuit, circuit simulation with the measured SAW-resonator S-parameters, and measurements of the dual-stage hybrid filter prototype. (b) Measured in-band group-delay response of the dual-stage hybrid filter prototype.

A comparison table with some related state-of-the-art filter designs is shown in Table I. As observed, the proposed low-cost hybrid filter has the following advantages. First, it avoids the use of well-paired/well-matched SAW resonators (at least two) as required in most of the traditional SAW-resonator-based filter developments [31]; thus, the current hybrid filter that uses a single-SAW BVD model has a much simpler design procedure and can even employ a commercial packaged acoustic resonator. Second, the use of the single external inductor per two-pole hybrid filter block simplifies the design process and makes it less time-lengthy/costly compared with other SAW-resonator-based filters for its accurate synthesis. Finally, the laminated multilayered implementation employed in its practical demonstration minimizes the filter footprint, which makes it a promising approach for an integrated-circuit development.

IV. Conclusion

A low-cost hybrid BPF device based on SAW resonators and external inductors and its design procedure have been presented. The engineered mixed-technology filter approach takes benefit from the small number of required circuit models, which ultimately results in a straightforward design strategy and miniaturized footprint. The suggested filter architecture is based on a dual-path coupling scheme that is matched to an equivalent classic transversal filter network through the even-/odd-mode analysis. The quality factors of the equivalent even- and odd-mode-subnetwork resonators have been studied, and their numerical results have been provided to illustrate the impact of the external inductor into them. Furthermore, two experimental single- and dual-stage BPF prototypes centered at 418 MHz have been built and tested for proof-of-concept purposes of the conceived hybrid filter design principle, showing a fairly close agreement between the measured and predicted results.

References

[1] C. Rauscher, “Microwave active filters based on transversal and recursive principles,” *IEEE Trans. Microw. Theory Techn.*, vol. MTT-33, no. 12, pp. 1350–1360, Dec. 1985.

[2] J. Rosenbaum, *Bulk Acoustic Wave Theory and Devices*. Norwood, MA, USA: Artech Print on Demand, 1988.

[3] A. Giménez, J. Verdú, and P. De Paco Sánchez, "General synthesis methodology for the design of acoustic wave ladder filters and duplexers," *IEEE Access*, vol. 6, pp. 47969–47979, 2018.

[4] Y. He *et al.*, "A direct matrix synthesis for in-line filters with transmission zeros generated by frequency-variant couplings," *IEEE Trans. Microw. Theory Techn.*, vol. 66, no. 4, pp. 1780–1789, Apr. 2018.

[5] S. Amari and G. Macchiarella, "Synthesis of inline filters with arbitrarily placed attenuation poles by using nonresonating nodes," *IEEE Trans. Microw. Theory Techn.*, vol. 53, no. 10, pp. 3075–3081, Oct. 2005.

[6] K. Nosaka, "Acoustic wave filter device, multiplexer, radio frequency front-end circuit, and communication device," U.S. Patent 20 190 181 833 A1, Jun. 13, 2019.

[7] K. Nosaka, "Acoustic wave filter device, radio-frequency front-end circuit, and communication apparatus," U.S. Patent 20 190 190 493 A1, Jun. 20, 2019.

[8] O. Ikata, T. Miyashita, T. Matsuda, T. Nishihara, and Y. Satoh, "Development of low-loss band-pass filters using SAW resonators for portable telephones," in *Proc. IEEE Ultrason. Symp.*, Oct. 1992, pp. 111–115.

[9] J. Liang, H. Zhang, D. Zhang, H. Zhang, and W. Pang, "Lamb wave AlN micromechanical filters integrated with on-chip capacitors for RF front-end architectures," *IEEE J. Electron Devices Soc.*, vol. 3, no. 4, pp. 361–364, Jul. 2015.

[10] D. Psychogiou, R. Gómez-García, R. Loeches-Sánchez, and D. Peroulis, "Hybrid acoustic-wave-lumped-element resonators (AWLRs) for high-Q bandpass filters with quasi-elliptic frequency response," *IEEE Trans. Microw. Theory Techn.*, vol. 63, no. 7, pp. 2233–2244, Jul. 2015.

[11] D. Psychogiou, R. Gómez-García, and D. Peroulis, "Single and multi-band acoustic-wave-lumped-element-resonator (AWLR) bandpass filters with reconfigurable transfer function," *IEEE Trans. Microw. Theory Techn.*, vol. 64, no. 12, pp. 4394–4404, Dec. 2016.

[12] Q. Yang, W. Pang, D. Zhang, and H. Zhang, "A modified lattice configuration design for compact wideband bulk acoustic wave filter applications," *Micromachines*, vol. 7, no. 8, p. 133, Aug. 2016.

[13] D. Psychogiou, R. Gómez-García, and D. Peroulis, "SAW-based bandpass filters with flat in-band group delay and enhanced fractional bandwidth," in *IEEE MTT-S Int. Microw. Symp. Dig.*, Sep. 2017, pp. 1–3.

[14] D. Psychogiou, R. Gómez-García, and D. Peroulis, "Coupling-matrix-based design of high-Q bandpass filters using acoustic-wave lumped-element resonator (AWLR) modules," *IEEE Trans. Microw. Theory Techn.*, vol. 63, no. 12, pp. 4319–4328, Dec. 2015.

[15] T. Makkonen, V. P. Plessky, S. Kondratiev, and M. M. Salomaa, "Electromagnetic modeling of package parasitics in SAW-duplexer," in *Proc. IEEE Ultrason. Symp.*, vol. 1, Nov. 1996, pp. 29–32.

[16] A. R. G. Bonastre, "RF filters and multiplexers based on acoustic wave technologies with ladder-type and cross-coupled topologies," Ph.D. dissertation, Dept. Telecommun. Syst. Eng., Auton. Univ. Barcelona, Spain, 2016.

[17] W. N. Allen, A. Gao, S. Gong, and D. Peroulis, "Hybrid bandpass-absorptive-bandstop magnetically coupled acoustic-wave-lumped-element-resonator filters," *IEEE Microw. Wireless Compon. Lett.*, vol. 28, no. 7, pp. 582–584, Jul. 2018.

[18] R. Gómez-García, D. Psychogiou, R. Loeches-Sánchez, and D. Peroulis, "Hybrid surface-acoustic-wave/microstrip signal-interference bandpass filters," *IET Microw., Antennas Propag.*, vol. 10, no. 4, pp. 426–434, Mar. 2016.

[19] X. Lu, K. Mouthaan, and T. S. Yeo, "A wideband bandpass filter with frequency selectivity controlled by SAW resonators," *IEEE Trans. Compon., Packag., Manuf. Technol.*, vol. 6, no. 6, pp. 897–905, Jun. 2016.

[20] D. Psychogiou, D. Peroulis, R. Loeches-Sánchez, and R. Gómez-García, "Analog signal-interference narrow-band bandpass filters with hybrid transmission-line/SAW-resonator transversal filtering sections," in *Proc. IEEE Int. Symp. Circuits Syst. (ISCAS)*, May 2015, pp. 281–284.

[21] D. Morgan, *Surface Acoustic Wave Filters: With Applications to Electronic Communications and Signal Processing*. London, U.K.: Academic, 2007.

[22] J. D. Larson, III, P. D. Bradley, S. Wartenberg, and R. C. Ruby, "Modified Butterworth-van Dyke circuit for FBAR resonators and automated measurement system," in *Proc. IEEE Ultrason. Symp.*, vol. 1, Oct. 2000, pp. 863–868.

[23] R. Zhang and L. Zhu, "Synthesis of dual-wideband bandpass filters with source-load coupling network," *IEEE Trans. Microw. Theory Techn.*, vol. 62, no. 3, pp. 441–449, Mar. 2014.

[24] R. Zhang, W. Yang, and D. Peroulis, "A new reconfigurable bandpass filter with adaptive resonators for switchable passband and in-band notch," in *Proc. IEEE Radio Wireless Symp. (RWS)*, May 2019, pp. 1–4.

[25] K. M. Lakin, G. R. Kline, and K. T. McCarron, "High-Q microwave acoustic resonators and filters," in *IEEE MTT-S Int. Microw. Symp. Dig.*, Jun. 1993, pp. 1517–1520.

[26] P.-Y. Chen, Y.-C. Chin, C.-Y. Chen, and C.-L. Hou, "Accurate formula for quality factor Q of thin film bulk acoustic resonators with close series and parallel resonance frequencies," in *Proc. 16th IEEE Int. Symp. Appl. Ferroelectr.*, May 2007, pp. 757–759.

[27] W. N. Allen, A. Gao, S. Gong, and D. Peroulis, "Simultaneous analog tuning of the series- and anti-resonances of acoustic wave resonators," in *Proc. IEEE 19th Wireless Microw. Technol. Conf. (WAMICON)*, Apr. 2018, pp. 1–3.

[28] R. Zhang and L. Zhu, "Synthesis and design of wideband dual-band bandpass filters with controllable in-band ripple factor and dual-band isolation," *IEEE Trans. Microw. Theory Techn.*, vol. 61, no. 5, pp. 1820–1828, May 2013.

[29] T.-C. Lee, A. Guyette, E. J. Naglich, and D. Peroulis, "Coupling-matrix-based SAW filter design," in *IEEE MTT-S Int. Microw. Symp. Dig.*, Jun. 2014, pp. 1–4.

[30] C. D. Nordquist *et al.*, "Inductive coupling for increased bandwidth of aluminum nitride contour-mode microresonator filters," in *IEEE MTT-S Int. Microw. Symp. Dig.*, May 2016, pp. 1–4.

[31] M. Kadota, T. Yoneda, K. Fujimoto, T. Nakao, and E. Takata, "Very small-sized resonator filter using shear horizontal wave on quartz," *Jpn. J. Appl. Phys.*, vol. 40, no. 5B, pp. 3718–3721, May 2001.

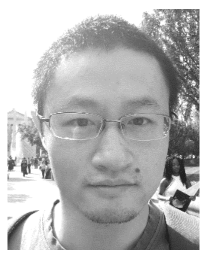

Runqi Zhang (Member, IEEE) received the B.Eng. and M.Eng. degrees in electromagnetic field and radio technology from the University of Electronic Science and Technology of China, Chengdu, China, in 2007 and 2010, respectively, and the Ph.D. degree from the School of Electrical and Electronic Engineering, Nanyang Technological University (NTU), Singapore, in 2015.

From 2014 to 2015, he was a Research Associate with the Centre for Infocomm Technology, NTU. From 2015 to 2016, he was a Research Engineer and then a Research Fellow with the Satellite and Airborne Radar Systems Laboratory, National University of Singapore, Singapore. From 2016 to 2019, he held a post-doctoral position at the Electrical and Computer Engineering, Purdue University, West Lafayette, IN, USA. Since October 2019, he has been a Senior BAW Filter Design Engineer with Akoustis, Inc., Huntersville, NC, USA. His current research interests include the satellite communication, synthesis and design of RF/microwave passive devices, surface-acoustic-wave (SAW)/BAW filter design, and LTCC application in the RF/microwave circuit.

Mahmoud Abdelfattah (Student Member, IEEE) received the B.S. degree in electrical engineering from the Princess Sumaya University for Technology, Amman, Jordan, in 2014, and the Ph.D. degree in electrical and computer engineering from Purdue University, West Lafayette, IN, USA, 2019.

He is currently a RF/EM Design Senior Engineer with Skyworks Solutions, Inc., Newbury Park, CA, USA. His current research interests include the design, manufacturing, and control of reconfigurable microwave and millimeter-wave cavity filters, lumped-element and planar filters, and microwave and millimeter-wave passive components.

Dr. Abdelfattah is also a member of the IEEE Microwave Theory and Techniques Society (IEEE MTT-S). He was a recipient of the IEEE WAMICON Best Paper in Conference Award in 2018 and the Second Place Award of the Student Design Competition on Switchable RF-MEMS Filter in the IEEE MTT-S IMS 2016.

Li Yang (Member, IEEE) received the M.Sc. degree in electrical and electronics engineering and the Ph.D. degree in electrical and computer engineering from the University of Macau (UM), Macau, China, in 2013 and 2018, respectively.

In 2018, he was a Research Associate with the Department of Electrical and Computer Engineering, UM. Since 2018, he has been holding a post-doctoral position at the Department of Signal Theory and Communications, University of Alcalá, Alcalá de Henares, Spain. His current research interests include the synthesis and design of RF/microwave planar and multilayered passive components.

Dr. Yang was a recipient of the Best Student Paper Award of the International Symposium on Antennas and Propagation 2010 in Macau.

Roberto Gómez-García (Senior Member, IEEE) was born in Madrid, Spain, in 1977. He received the degree in telecommunication engineering and the Ph.D. degree in electrical and electronic engineering from the Polytechnic University of Madrid, Madrid, in 2001 and 2006, respectively.

He was an Adjunct Part-Time Professor with the University of Electronic Science and Technology of China, Chengdu, China, from 2017 to 2019, and an Invited Visiting Professor with the Gdańsk University of Technology, Gdańsk, Poland, from 2018 to 2019. Since 2006, he has been an Associate Professor with the Department of Signal Theory and Communications, University of Alcalá, Alcalá de Henares, Spain. He has been, for several research stays, with the C2S2 Department, XLIM Research Institute, University of Limoges, Limoges, France, the Telecommunications Institute, University of Aveiro, Aveiro, Portugal, the U.S. Naval Research Laboratory, Microwave Technology Branch, Washington, DC, USA, and Purdue University, West Lafayette, IN, USA. His current research interests include the design of fixed/tunable high-frequency filters and multiplexers in planar, hybrid, monolithic microwave-integrated circuit technologies, multifunction circuits and systems, and software-defined radio and radar architectures for telecommunications, remote sensing, and biomedical applications, in which he has authored/coauthored around 95 journal articles (75 in IEEE journals and 35 as the first author) and 135 conference papers.

Dr. Gómez-García also serves as a member of the Technical Review Board for several IEEE and EuMA conferences. He is also a member of the IEEE MTT-S Filters (MTT-5), the IEEE MTT-S RF MEMS and Microwave Acoustics (MTT-6), the IEEE MTT-S Wireless Communications (MTT-23), the IEEE MTT-S Biological Effects and Medical Applications of RF and Microwave (MTT-28), and the IEEE CAS-S Analog Signal Processing Technical Committees. He was a recipient of the 2016 IEEE Microwave Theory and Techniques Society (MTT-S) Outstanding Young Engineer Award. He was named an IEEE Circuits and Systems Society Distinguished Lecturer for the term 2020–2021. He was an Associate Editor of the IEEE TRANSACTIONS ON MICROWAVE THEORY AND TECHNIQUES from 2012 to 2016 and the IEEE TRANSACTIONS ON CIRCUITS AND SYSTEMS I: REGULAR PAPERS from 2012 to 2015, a Senior Editor of the IEEE JOURNAL ON EMERGING AND SELECTED TOPICS IN CIRCUITS AND SYSTEMS from 2016 to 2017, and a Guest Editor of the 2013 and 2018 IEEE JOURNAL ON EMERGING AND SELECTED TOPICS IN CIRCUITS AND SYSTEMS Special Issue on Advanced Circuits and Systems for CR/SDR Applications and Special Issue on Wireless Sensing Circuits and Systems for Healthcare and Biomedical Applications, the *IET Microwaves, Antennas, and Propagation* 2013 "Special Issue on Advanced Tunable/Reconfigurable and Multi-Function RF/Microwave Filtering Devices," and the *IEEE Microwave Magazine* 2014 Special Issue on Recent Trends on RF/Microwave Tunable Filter Design and 2019 Special Issue on Wireless Sensors for Biomedical Applications. He is also an Associate Editor of the IEEE MICROWAVE AND WIRELESS COMPONENTS LETTERS, the IEEE JOURNAL OF ELECTROMAGNETICS, RF AND MICROWAVES IN MEDICINE AND BIOLOGY, IEEE ACCESS, the *IET Microwaves, Antennas & Propagation*, and the *International Journal of Microwave and Wireless Technologies*. He is also a reviewer for several IEEE, IET, EuMA, and Wiley journals.

Dimitrios Peroulis (Fellow, IEEE) received the Ph.D. degree in electrical engineering from the University of Michigan, Ann Arbor, MI, USA, in 2003.

He is currently the Reilly Professor and the Michael and Katherine Birck Head of the School of Electrical and Computer Engineering, Purdue University, West Lafayette, IN, USA. He has coauthored over 380 journal articles and conference papers. His research interests are focused on the areas of reconfigurable systems, cold-plasma RF electronics, and wireless sensors. He has been a key contributor in developing high-quality widely tunable filters and novel filter architectures based on miniaturized high-Q cavity-based resonators in the 1–100-GHz range. He is also leading research efforts in high-power multifunctional RF electronics based on cold-plasma technologies.

Dr. Peroulis received the National Science Foundation CAREER Award in 2008. He received the "Tatsuo Itoh" Award in 2019 and the Outstanding Young Engineer Award in 2014 from the IEEE Microwave Theory and Techniques Society (MTT-S). In 2012, he received the Outstanding Paper Award from the IEEE Ultrasonics, Ferroelectrics, and Frequency Control Society (Ferroelectrics Section). His students have received numerous student paper awards and other student research-based scholarships. He has been a Purdue University Faculty Scholar and received ten teaching awards, including the 2010 HKN C. Holmes MacDonald Outstanding Teaching Award and the 2010 Charles B. Murphy Award, which is Purdue University's highest undergraduate teaching honor.